PERGAMON

Continental Shelf Research 22 (2002) 859–880

CONTINENTAL SHELF RESEARCH

www.elsevier.com/locate/csr

Spatial and temporal distribution of contaminated, effluent-affected sediment on the Palos Verdes margin, southern California

Homa J. Lee[a,*], Christopher R. Sherwood[a], David E. Drake[b], Brian D. Edwards[a], Florence Wong[a], Michael Hamer[c]

[a] *US Geological Survey, 345 Middlefield Rd., Mail Stop 999, Menlo Park, CA 94025, USA*
[b] *Drake Marine Consulting, Ben Lomond, CA 95005, USA*
[c] *City of San Leandro, San Leandro, CA 94577, USA*

Received 4 June 2000; accepted 12 December 2001

Abstract

A sedimentary deposit on the continental margin near the Palos Verdes Peninsula, California is comprised of sewage effluent and geologic materials and is contaminated with metals, pesticides (including DDT and associated compounds), and PCBs. The deposit was mapped with subbottom acoustic profilers, and sediment cores were analyzed for geochemical and physical properties to determine the volume of the deposit and the distribution and mass of contaminants. Mapping showed that the deposit ranges up to 60-cm thick, has a total volume exceeding 9 million m^3, and covers over 40 km^2. Virtually the entire effluent-affected deposit is contaminated with DDT and PCBs. Nearly half of the area of the deposit lies on the continental slope, but 70–75% of the volume of the deposit and total mass of DDT reside on the continental shelf. Analysis of data collected biennially since 1981 by the Sanitation Districts of Los Angeles County show that the mass of DDT has apparently decreased at some stations but has remained essentially constant at others. Temporal changes in mass per unit area of DDT are not statistically significant (at the 90% confidence level) at the most contaminated locations over a 16-yr period. The results of this mapping effort were used as a basis for modeling efforts described elsewhere in this issue.

Keywords: Shelf sediment; Pollution; Mapping; California; DDT; PCBs

1. Introduction

The Palos Verdes Hills and Peninsula are a part of the greater Los Angeles metropolitan area (Fig. 1). The continental margin south of the peninsula has a narrow shelf and slope and has been the recipient of wastewater discharged through the Whites Point outfall for over 60 years. Solid particles carried by the wastewater have mixed with geologic materials to produce an effluent-affected sediment deposit that is contaminated with a variety of substances from residences and industries that contribute to the sewer system of Los Angeles County. Among these contributors

*Corresponding author. Tel.: +1-650-329-5485; fax: +1-650-329-5411.

E-mail address: hjlee@usgs.gov (H.J. Lee).

0278-4343/02/$ - see front matter
PII: S0278-4343(01)00108-X

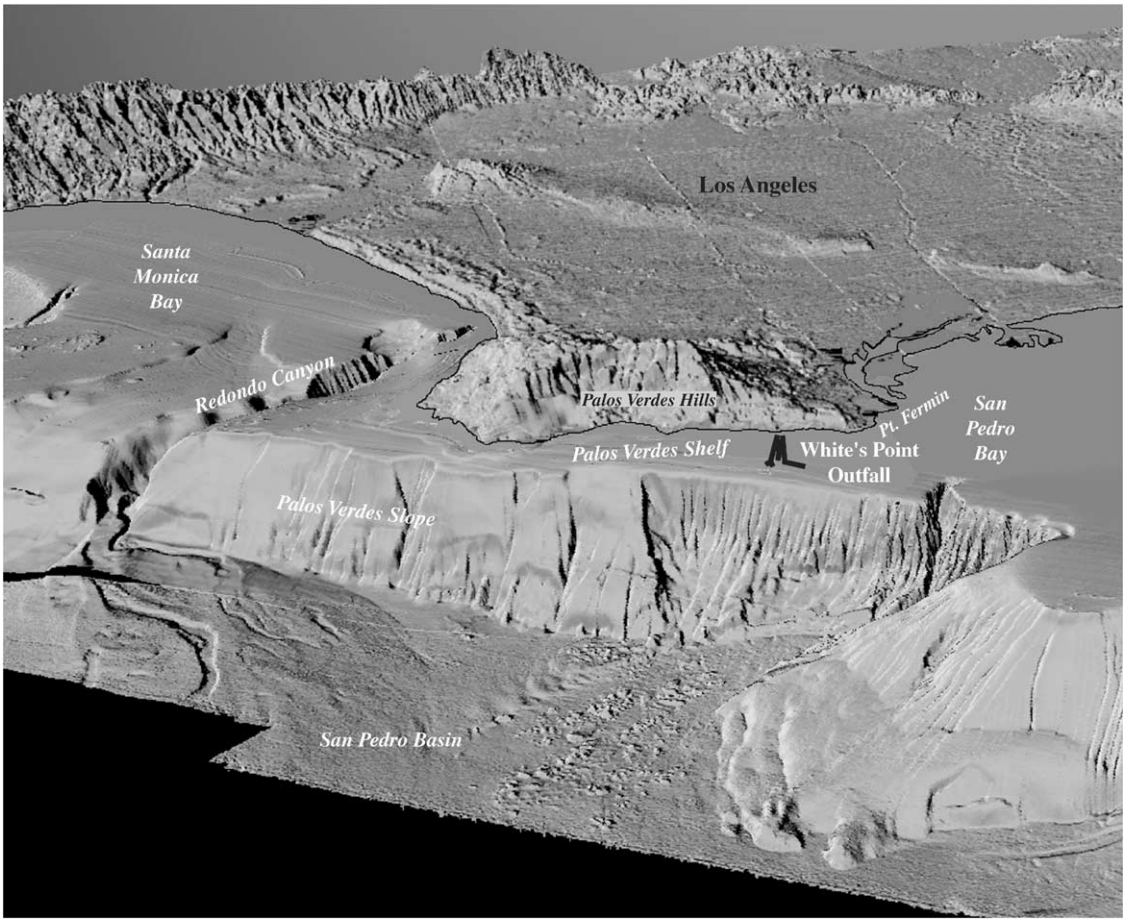

Fig. 1. Oblique view of the Palos Verdes margin based on multi-beam bathymetry, showing features discussed in the text (courtesy of J.V. Gardner and P. Dartnell, US Geological Survey).

was a large manufacturing plant that produced dichlorodiphenyltrichloroethane (DDT) before it was banned in the US, and other plants that delivered polychlorinated biphenyls (PCBs). Because DDT has been linked to severe reproductive problems in birds and other wildlife, and cancer in humans, there has been considerable concern regarding the presence of a DDT-contaminated deposit on the Palos Verdes margin. Specifically, there has been interest in determining (1) how much DDT is still retained in the sediment and what volume of sediment is contaminated, (2) how the DDT is distributed areally and with depth in the sediment column, and (3) whether geologic, biologic, and chemical processes are reducing the bioavailability of DDT and its byproducts. To determine the characteristics of this contaminated, effluent-affected sediment deposit and to predict the fate of the deposit if no remedial actions are taken (natural recovery), the USGS and cooperative researchers conducted a large, multidisciplinary investigation. Many of the papers in this issue describe work conducted as part of this investigation. The present paper describes one part of this study: an effort to map the deposit in three dimensions through time using a variety of techniques and to quantify the extent and magnitude of DDT- and PCB-contamination. The results include an analysis of temporal trends in contamination data at several sites, calculation of

total mass of DDT and PCBs contained in the sediment, a presentation of the surface area (footprint) of contaminated sediment, and a basis for predicting the natural recovery of the deposit.

2. Background

2.1. Geologic setting

The Palos Verdes Peninsula is principally composed of seaward-dipping siliceous shales and volcanic rocks of the Altamira member of the Miocene Monterey Formation (Conrad and Ehlig, 1987). The adjacent shelf is narrow (typically 2–4 km; 5 km wide at its widest point south of Point Fermin) and shallow (shelf break at 75 m). Seaward of the shelf break, the continental slope is unusually narrow (approximately 3 km) and steep (mean steepness of about 13°). The continental slope abruptly terminates at the nearly flat 800-m-deep floor of San Pedro Basin. The slope is marked by numerous gullies and shallow-seated landslides, as well as several large, deep-seated failures (Hampton et al., 1996; Lee et al., 2000). The shelf is underlain by truncated, seaward-dipping strata, assumed to be units of the Monterey Formation (Moore, 1960). This submerged rock platform is unconformably overlain by unconsolidated sedimentary layers with thickness ranging from a few meters in shallow water along the coast and at the northwest end of the shelf, to about 32 m on the outer shelf southwest of Point Fermin (Pierson et al., 1987; Fischer and Lee, 1992; Hampton et al., 2002). These strata are assumed to contain post-glacial sediment deposited during and after the most recent (post-Wisconsin) rise in sea level. The strata on the outer shelf form a narrow elongate wedge that thins from about 32 m in thickness on its eastern end to about 5 m in thickness south of Pt. Vicente (Hampton et al., 2002), implying that: (1) much of the sediment that formed the post-transgressive layers on Palos Verdes shelf came from San Pedro shelf to the southeast (Kolpack, 1987), and (2) that net transport by ocean currents was directed alongshelf toward the northwest, as they are today (Hickey, 1992; Noble et al., 2002).

2.2. Sources of sediment

As a veneer lying atop the post-transgressive, native sediment, the effluent-affected layer consists of organic-rich sand, silt, and clay particles derived from both natural and anthropogenic sources. Natural sources include local cliffs, the San Pedro shelf, and the urban rivers of the Los Angeles basin (Kolpack, 1987). Anthropogenic sources include the Whites Point outfall and the Portuguese Bend landslide (PBL, Fig. 2). We consider the PBL an anthropogenic source because rapid movement of part of an ancient landslide complex was initiated in 1956 by road construction (Merriam, 1960; Kayen et al., 2002), and engineering measures largely halted the landslide in 1988. Estimates of the contribution of sediment from the PBL have been calculated from its geometry and measured rate of advance (Ehlig, pers. comm.; Kayen et al., 2002). The PBL has contributed between 6 and 9 million mt of terrigenous, essentially uncontaminated sediment to the inner shelf, and there is textural, minerological, and chemical evidence that a significant volume of PBL-derived sediment is incorporated in the effluent-affected deposit (Wong, 2002; Kayen et al., 2002).

Wong (2002) showed that the mineralogy of the fine sand in the effluent-affected layer and in the native sediment below it on the southeastern end of the Palos Verdes shelf is characterized by a hornblende and epidote assemblage typical of the mineralogy of modern shelf sands on a regional scale in the southern California borderland. The dominance here of this assemblage and relative dearth of material reflecting local coastal mineralogy implies that native sediment on the mid- to outer shelf has the same source as that on the San Pedro Shelf, i.e., the Los Angeles, San Gabriel, and Santa Ana Rivers. Mineralogic evidence also indicates that locally derived sand dominates on the inner shelf and to depths up to about 60 m only on the western end of the Palos Verdes margin. Under modern conditions, significant sediment transport to the Palos Verdes shelf from the northwest is severely restricted by the shelf circulation patterns (Noble et al., 2002) and by the Redondo Submarine Canyon, which cuts

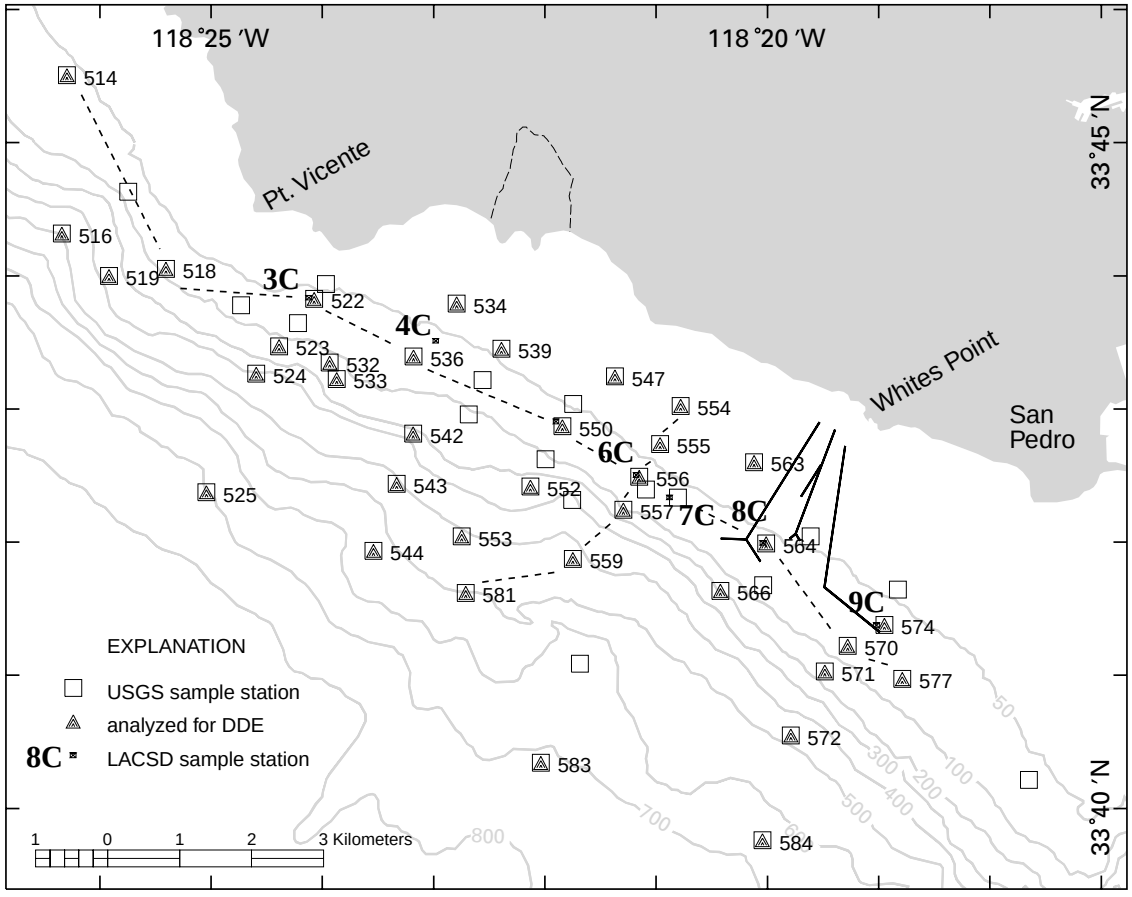

Fig. 2. Locations of coring stations occupied as part of this study and LACSD core stations referred to in this paper. Lines of cores used to develop the profiles of Fig. 4 are identified.

across the southeastern end of Santa Monica Bay into shallow water (Fig. 1; Gardner et al., 1999a) and intercepts sediment moving southeastward on the inner shelf (Emery, 1960; Rice et al., 1976). Modern sand supply to the Palos Verdes shelf from the southeast (San Pedro shelf) is inferred to be small because it is intercepted by an exposed bedrock ridge, which traces the submarine extension of the Cabrillo fault system (Gardner et al., 1999b).

2.3. History of wastewater discharge

The Sanitation Districts of Los Angeles County (LACSD) in 1937 began to discharge treated municipal and industrial wastewater from the Joint Water Pollution Control Plant (JWPCP) through a 1.5-m diameter ocean outfall near Whites Point at a water depth of 34 m (Stull et al., 1996). A 1.8-m outfall was added in 1947 with a terminus at a depth of 34 m, to which a diffuser ending at a depth of 49 m was added in 1953. In 1956 and 1966, two more outfalls with diameters of 2.3 and 3.0 m and Y- and L-shaped diffusers, terminating at depths of ~64 and 58 m, respectively, were constructed to accommodate increased discharges. Use of the original 34-m outfall was discontinued in 1958, and the modified 49-m outfall has only been used for emergencies since 1966. Wastewater and suspended-solids

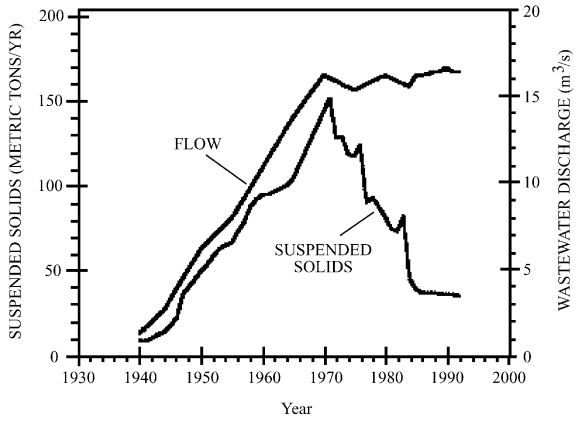

Fig. 3. Discharges of wastewater (in m^3/s) and suspended solids (in dry metric tons/year) from the Whites Point ocean outfall system (LACSD, 1992).

discharge peaked in 1971, and have decreased since implementation of improved water-conservation and treatment measures (Fig. 3). The JWPCP effluent discharged before 1970 contained a variety of contaminants, including trace metals and chlorinated hydrocarbons, such as DDT and PCBs. Source-control and treatment strategies begun in 1970 led to a rapid decrease in the discharge rate of some contaminants (e.g., DDT and PCBs) during the 1970s and early 1980s, and a less rapid, but still substantial, decline in the suspended-solids emission rate. In 1971, DDT discharge was measured at about 21 mt/yr but, by 1987, DDT discharge had declined to 0.03 mt/yr. Suspended-solids discharge was reduced to about 40,000 mt/yr by 1985, and it has remained between 30,000 and 40,000 mt/yr through 1994 (Fig. 3; LACSD, 1992). The total discharge of suspended solids from 1937 to 1995 has been about 4.1 million mt.

2.4. LACSD monitoring

As part of their monitoring program, the Sanitation Districts of Los Angeles County established a sampling grid that extends along the Palos Verdes margin from a point just south of Redondo Canyon to near Point Fermin. High quality gravity cores (Bascomb et al., 1982), have been taken biennially since 1981 at stations within the grid. Not all stations are sampled during each biennial program, but a few have been sampled every time. Several stations (Sites 3C–9C; Fig. 2) along the 60-m isobath, where the effluent-affected deposit is thickest, provide a good record of temporal changes in surface concentrations, total mass per unit area, and vertical distribution of *p,p′*-DDE (the dominant DDT isomer). LACSD (1992, 1998) described their sampling program and analyses methods. Except for a few early cores, LACSD analyzed most cores at 2-cm intervals and reported water content, wet bulk density, and *p,p′*-DDE concentration.

2.5. Background sedimentation rate

Knowledge of the background (or "natural") sedimentation rate is important because it provides a context for evaluating accumulation rates of anthropogenic materials. Background sedimentation rate is also required for modeling long-term accumulation or erosion of the effluent-affected deposit (e.g., Sherwood et al., 2002). As defined here, the background rate is the rate at which sediment would accumulate under present-day conditions on the outer Palos Verdes shelf, in the absence of contributions from the PBL or the JWPCP. Kolpack (1987) and Hampton et al. (2002) used high-resolution seismic reflection data collected by Moore (1960), Pierson et al. (1987), Fischer and Lee (1992), Hampton et al. (2002) to estimate long-term (10,000–15,000-yr) accumulation rates ranging from <0.1 cm/yr on the inner shelf to a maximum of about 0.3 cm/yr on the outer shelf south of Point Fermin (Hampton et al., 2002), depending on the age assigned to the strata. At two sites we discuss in detail in later sections (LACSD Sites 3C and 6C, Fig. 2), these rates would be approximately 0.1 and 0.2 cm/yr, respectively. These rates average over thousands of years of sea-level rise and highstand conditions, during which episodic tectonic activity, climate change, and shifts in magnitude and location of important local and regional sediment sources have likely occurred.

Profiles of the radioactive decay product ^{210}Pb determined from cores obtained at LACSD Site 6C (Wheatcroft and Martin, 1996) and at Sites 3C,

6C and 6CD (Swift et al., 1996) were used to estimate deposition rates in pre-effluent sediment. The profiles indicate that sediment in a layer approximately 10 cm thick, lying below the effluent-affected deposit, accumulated at about 0.2 cm/yr on the outer part of Palos Verdes shelf. The estimates assume a constant rate of sediment and ^{210}Pb supply, which is probably reasonable during the relevant period (ca. 1890–1940), prior to significant discharges from the JWPCP or recent movement of the PBL.

These long-term, pre-effluent estimates probably represent upper bounds on the modern-day background sedimentation rate. First, our definition of background sedimentation rate specifically excludes contributions from the PBL, although it has likely contributed to the long-term estimate. Second, the major regional rivers, including the Los Angeles, San Gabriel, and Santa Ana, which are a likely source of fine sediment, were extensively modified (Brownlie and Taylor, 1981; Inman and Jenkins, 1999) by construction of flood-control basins and reservoirs in the 1930s–1950s. Finally, the breakwater for the Port of Los Angeles—Long Beach (constructed in 1937) has formed a trap for some of the sediment delivered to the coast by the Los Angeles River. Material dredged from the harbor is placed in deepwater disposal where it cannot supply material to the Palos Verdes shelf. In summary, because all indications are that the natural sediment supply has not increased, and has likely decreased since the 1930s–1940s, the present-day background sedimentation rate is likely somewhat <0.2 cm/yr.

3. Methods

The geometry and character of the effluent-affected sediment deposit were determined using acoustic surveying instruments and physical and chemical analysis of bottom sediment samples collected during USGS research cruises in the summer of 1992 and provide a detailed snapshot of the effluent-affected deposit at that time. The acoustic instruments included a very-high-resolution seismic-reflection profiler (chirp) and a high-resolution 3.5-kHz seismic-reflection profiler. The chirp, which has a vertical resolution of 20 cm, was used to map sediment thicknesses on the order of a few tens of centimeters to a few meters. The 3.5-kHz profiler was used to map sediment thicknesses on the order of a few meters to several tens of meters. The details of these surveys are presented by Hampton et al. (2002).

Sediment samples were collected to: (1) obtain detailed measurements of the thickness of the effluent-affected sediment deposit and the distribution of DDT and PCBs in the upper meter of the sediment column; (2) provide information about sedimentation processes on the shelf, slope, and basin-fan as they relate to transport pathways and subsequent depositional sites; (3) obtain information on sedimentation rates in the region immediately before and during industrialization; and (4) determine geotechnical properties for use in predicting gravity-driven sediment transport processes. Navigation for all aspects of this investigation was by differential GPS. We based our core-station locations partly on the sampling grid established by the LACSD and partly on results of our acoustic survey. Many of the stations were selected on the basis of chirp sonar records (Hampton et al., 2002), which disclosed a surficial sedimentary unit to the west of the outfall pipes that is clearly the effluent-affected sedimentary deposit. Six offshore-trending transects with about six coring stations per transect were selected along chirp lines. Stations were positioned to sample the main part of the effluent-affected sediment unit, as well as both landward and seaward transition zones. An attempt was made to reoccupy a number of the LACSD stations on the shelf and upper slope so that 1992 concentrations of DDT and PCBs could be related to earlier and later measurements.

Samples of most stations were obtained with a standard Naval Electronics Laboratory (NEL) box corer, which has a surface area of $20\,\text{cm} \times 30\,\text{cm}$ and can penetrate up to 60 cm (Rosfelder and Marshall, 1967). A shipboard subsampling device was used on the box sample to obtain an 8.5-cm-diameter cylindrical subcore of the sediment mass. The device has a fixed piston that maintains the sediment surface and is intended to prevent internal distortion and loss

of subbottom depth reference within the subcores. Two or three subcores were obtained from every box. At several locations near the 60-m-isobath, the box corer did not penetrate all the way through the low-density surface layer that corresponds to the effluent-affected sediment. At each of these locations, 2 cores were also obtained with a gravity corer that is capable of greater penetration than the box corer.

Gravity corers are known to incompletely sample the surface of the sediment column, mainly because of the presence of a "fingers" type core retainer at the bottom of the corer that opens only when the sediment strength exceeds a threshold value. Accordingly, at these thick effluent-affected sediment layer locations, two types of sediment cores are available: (1) high-quality subcores of box core samples from the upper 45-cm of the sediment column, and (2) poorer quality gravity cores that sample into native sediment below the effluent-affected sediment layer but that imperfectly sample the sediment surface. All cylindrical core samples were logged at 1-cm spacing for density using the gamma-ray-attenuation method, acoustic velocity, and magnetic susceptibility (Kayen and Phi, 1997; Kayen et al., 1999). To create continuous logs of the complete effluent-affected sediment layer, box core and gravity core density logs were matched. The entire gravity core density profile was shifted downward relative to the density log for the associated box core until the best correspondence between the two density logs was obtained. The amount of downward shifting (corrected depth reference) ranged from 6 to 18 cm. These corrected depth references were applied to all measurements conducted on gravity core samples.

4. Distribution of contaminants, USGS survey, 1992

Core samples from 38 stations were tested for DDT, PCBs, and total organic carbon (TOC) content. Samples from 13 stations were tested using 2-cm core increments, and samples from the remainder were tested using 4-cm core increments. A discussion of laboratory measurement and sampling variability as well as variability between replicate box cores is given by Murray et al. (2002). In the continuing LACSD sediment sampling and analysis program, *p,p′*-DDE was selected as a representative for Palos Verdes sediment contaminants. We also selected *p,p′*-DDE to represent DDT contamination for comparison with previous studies and because *p,p′*-DDE is the dominant metabolite of DDT found in shelf sediment.

4.1. *p,p′-DDE distribution*

p,p′-DDE profiles from cores located along two lines (a shore normal line and one approximately aligned with the 60-m isobath; Fig. 2) were assembled to produce cross sections (Fig. 4). The depth reference in the gravity cores has been shifted downward to match the box cores, as described above. The shore-parallel profile (Fig. 4b) shows a sedimentary deposit that is contaminated with *p,p′*-DDE over a distance of at least 15 km along the Palos Verdes margin. Contamination levels in excess of 1 ppm extend to over 50 cm in the sediment column, and the major part of the contaminated sediment body lies to the northwest of the outfall discharge point. Sediment transport to the northwest is consistent with current meter measurements (Noble et al., 2002). Highest concentration levels (in excess of 200 ppm) are found below 30 cm depth in the sediment, and concentration levels of 5–10 ppm exist at the sediment surface at many locations. The highest concentration levels reflect the period when onshore industrial production of DDT was active, prior to the early 1970s. Mixing of this highly contaminated sediment with more recently deposited, less contaminated sediment is most likely a result of biological processes (Wheatcroft and Martin, 1996; Sherwood et al., 2002). These mixing processes lead to the significant contamination levels that still exist at the seafloor surface.

The shore-perpendicular profile (Fig. 4a) shows that the highest levels of *p,p′*-DDE contamination are below 30 cm depth in the sediment column near our station 556, which lies near the depth at which the diffuser pipes discharge (roughly 60 m). The thickness of sediment containing *p,p′*-DDE concentrations in excess of 1 ppm thins to <20 cm

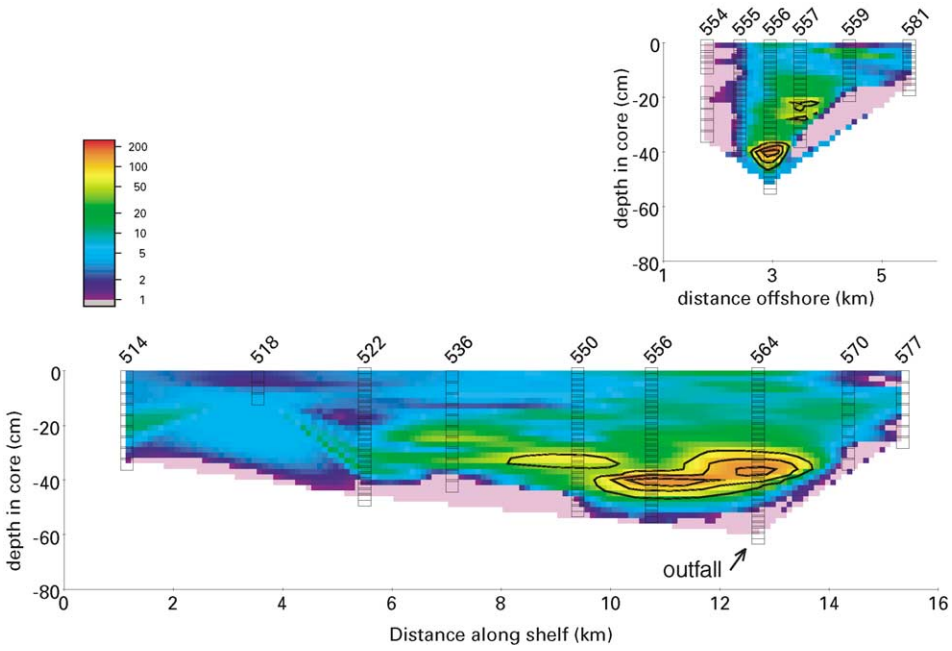

Fig. 4. (a) Profile of *p,p′*-DDE concentration along a shore parallel line (see Fig. 2 for location). (b) Profile of *p,p′*-DDE concentration along a shore normal line (see Fig. 2 for location).

on the mid slope, and the depth in sediment to the maximum concentration of *p,p′*-DDE decreases. A result is that the sediment on the slope has relatively high surface concentrations even though the thickness of *p,p′*-DDE-impacted sediment is much less. Proceeding shoreward from the 60 m isobath, the thickness of sediment impacted by *p,p′*-DDE does not thin appreciably although concentration levels decrease rapidly. A likely explanation is that concentration levels decrease because the sediment grain size increases and *p,p′*-DDE is typically associated with the fine fraction.

The contouring routines of a commonly used geographic information system (GIS) application (ArcInfo©) were used to develop isopleths of *p,p′*-DDE concentrations in the surface sediment (0–4 cm). The software was applied to calculate the areas within the 1-, 5-, and 10-ppm *p,p′*-DDE isopleths (Fig. 5, Table 1). The displayed data are contoured only within the area defined by the sampling stations. Accordingly, the isopleths (1 and 5 ppm) that cross the boundary of the area mapped are not constrained. Because virtually all of the area mapped has surface concentrations of *p,p′*-DDE greater than 1 ppm, the total area lying within the 1 ppm isopleth is likely much greater than the 43.1 km^2 given in the table. The 5 ppm isopleths are better constrained and define two areas, one that extends from about 1 km ESE of the outfall to a point near Portuguese Bend and another that exists south of Long Point. This concentration level begins in about 45 m of water and extends down the continental slope to water depths greater than 300 m. The 12.6 km^2 area shown for this 5 ppm surface concentration level is probably only slightly less than the area would be if the sampling area were extended. The 10 ppm isopleth is constrained, and the 3.4 km^2 area given is a good representation of the area that is contaminated at this concentration. Surface concentrations greater than 10 ppm exist within about 2 km of the outfall.

The surface *p,p′*-DDE footprint is also categorized according to water depth in Table 1. About 56% of the sediment with a surface concentration greater than 10 ppm is found in water depths

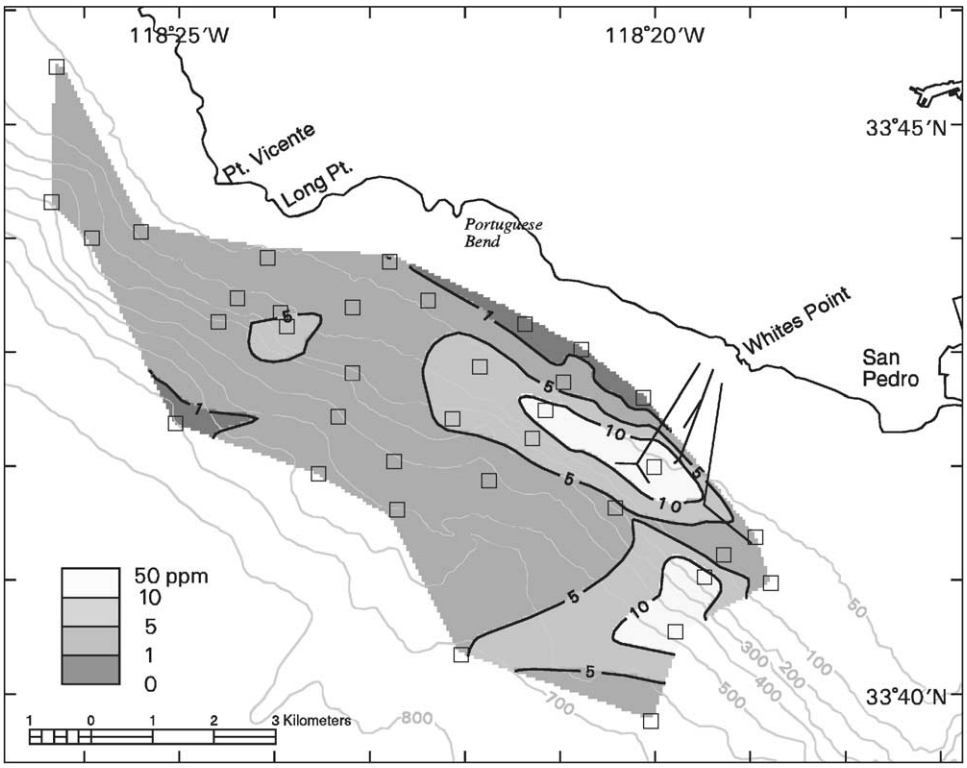

Fig. 5. *p,p′*-DDE footprint based on concentration measurements in the upper 4 cm.

Table 1
Characteristics of the effluent-affected sediment layer calculated using core data and a geographic information system

Water depth (m)	Area in which the surface concentration of *p,p′*-DDE exceeds 1 ppm (km^2)	Area in which the surface concentration of *p,p′*-DDE exceeds 5 ppm (km^2)	Area in which the surface concentration of *p,p′*-DDE exceeds 10 ppm (km^2)	Integrated mass of *p,p′*-DDE (mt)	Volume (million m^3)-from density logs
30–60	6.0	2.2	1.0	24.7	4.3
60–100	7.8	2.9	0.9	26.1	2.3
100–200	4.8	1.9	0.3	6.1	0.8
200–400	8.2	1.8	0.5	5.1	1.2
>400	16.3	3.8	0.7	4.8	1.2
Total	43.1	12.6	3.4	66.8	9.8

<100 m (near to or somewhat deeper than the continental shelf break), and the remainder is found in greater water depths (continental slope). About 40% of the sediment with a surface concentration greater than 5 ppm is found in water depths <100 m, and the remainder lies on the continental slope.

The distributions of *p,p′*-DDE, total DDT, total PCBs, and TOC show similar patterns. The zones of highest concentration extend from slightly SE of

the outfall pipes to several kilometers NW of the pipes. The highest concentrations are typically centered on the 60-m isobath. Concentrations decrease both inshore and offshore of this isobath but relatively high concentrations extend across the shelf break and onto the upper slope.

4.2. Mass of p,p′-DDE per unit area (inventory)

The accumulated mass of p,p'-DDE per unit area is the total mass of p,p'-DDE that lies below a unit area of the seafloor. Within any slice of core, the mass per unit area of p,p'-DDE is the concentration of p,p'-DDE (mass of p,p'-DDE per unit mass of dry sediment grains) multiplied by the dry density of the sediment (mass of dry sediment grains per unit volume of bulk sediment, including pore space) and the length of the slice. Summing the mass per unit area of all slices for a given core gives the accumulated mass of p,p'-DDE per unit area for that core. If the core penetrated all the way through the effluent-affected layer, then this calculated accumulated mass per unit area represents the total mass per unit area; otherwise it is a lower bound. The dry density of sediment was calculated from the sediment water content and available bulk densities using the formula (Lambe and Whitman, 1969):

$$\text{Dry density} = \text{bulk density}/(1 + \text{water content}).$$

Note that water content is given by the engineering definition: weight of water divided by weight of dry solids. A comparable definition is

$$\text{Dry density} = \text{grain density} \times (\text{1-porosity}).$$

The accumulated mass per unit area of p,p'-DDE was calculated for all cores analyzed for geochemistry in our study. Their variations over the Palos Verdes margin are shown in Fig. 6. The routines within ArcInfo© were used to integrate the values displayed in Fig. 6 to obtain estimates of total mass of p,p'-DDE as a function of water depth over the mapped part of the margin. These integrated values (Table 1) indicate that the total mass of p,p'-DDE for the area mapped is 66.8 mt and that about 75% of the total mass lies in water depths <100 m. Similar maps were prepared for total DDT, total PCBs, and TOC. The data show a strong association between the mass per unit areas of p,p'-DDE, total DDT, total PCBs, and TOC. Murray et al. (2002) document excellent spatial correlations between total DDT and p,p'-DDE, and between total PCBs and p,p'-DDE (correlation coefficients of 0.97 and 0.99, respectively).

Murray et al. (2002) present the results of a geostatistical study that evaluates the distribution of the accumulated mass per unit area of p,p'-DDE in the study area. Conditional sequential simulation was used to derive 100 equiprobable maps. These maps were analyzed statistically to obtain the expected values of the distribution of the mass per unit area at regularly spaced grid nodes in the map area (Murray et al., 2002). The maps of the expected values were integrated to yield a total mass of p,p'-DDE of 72 mt. This result was obtained over an area of 22.1 km^2. A total of 87–88% of this integrated mass is in water depths of <100 m. This total mass value compares favorably with the value of 66.8 mt obtained using contoured core data and a direct integration within ArcInfo©, as discussed above.

5. Temporal changes in the effluent-affected sediment deposit, LACSD surveys

Temporal trends in the concentration, mass, and vertical distribution of p,p'-DDE are used to make inferences regarding processes affecting the deposit, as discussed by Sherwood et al. (2002). The evolution of a cross-section along the 60-m isobath of p,p'-DDE concentrations reported by LACSD is depicted in Fig. 7. In this plot, dashed lines indicate the alongshelf location of gravity cores, and p,p'-DDE concentrations are contoured. The depth in each core at which p,p'-DDE concentrations fall to 1 ppm is used as a datum to approximately represent the surface of pre-effluent sediment. In this relative coordinate system, the deposit appears as a positive feature, and the vertical axis provides an approximation of its thickness. The large vertical exaggeration ($4000\times$) helps highlight the asymmetrical shape of the deposit, which thins rapidly toward the southeast

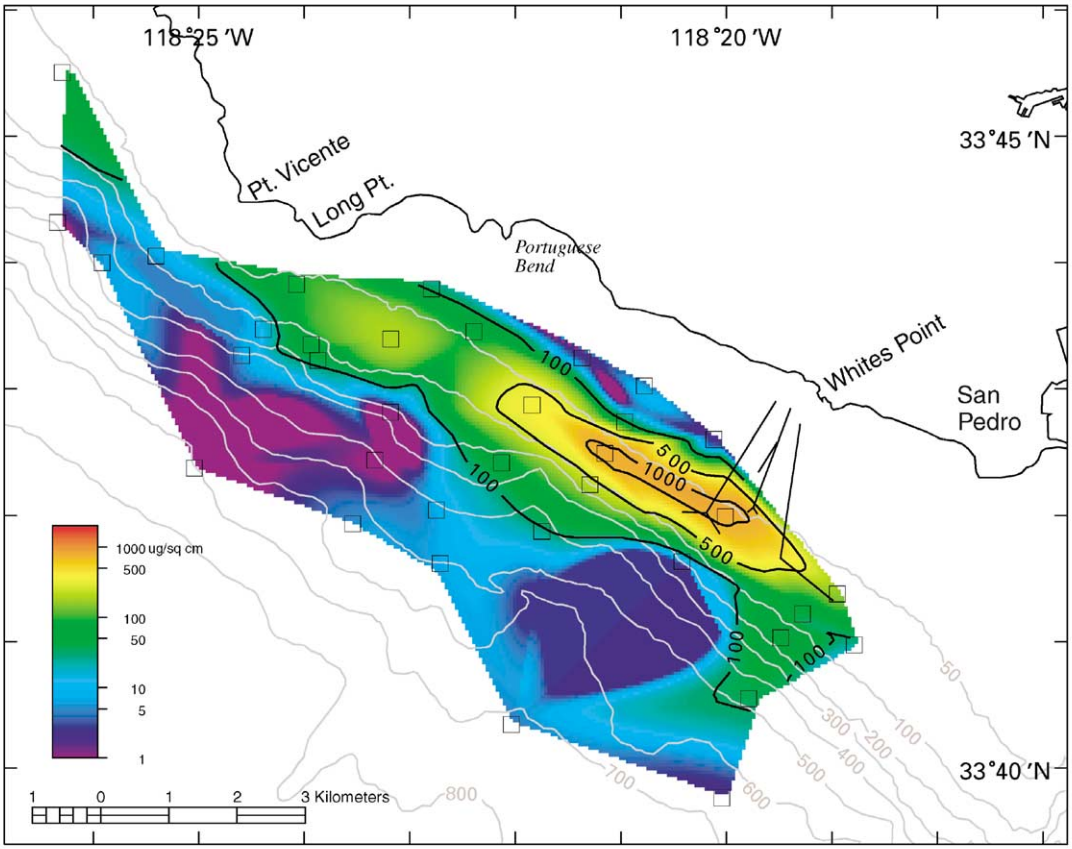

Fig. 6. Distribution of mass per unit area of *p,p′*-DDE obtained from core samples.

(between Sites 8C and 9C) but only gradually toward the northwest (from 6C to 3C). Also apparent is the accumulation of material on the northwest portion of the deposit (vicinity of Sites 3C, 4C, and 5C) with relatively low concentrations of *p,p′*-DDE. In the SE portion of the deposit (Sites 6C, 8C, and 9C), high concentrations of *p,p′*-DDE have persisted since 1981. The region southeast of Site 9C appears mostly non-depositional.

Temporal trends were quantified by tracking changes in surface concentrations (top 2 cm) and mass per unit area at LACSD stations 3C, 6C, and 8C (Fig. 8). Surface concentrations were taken directly from LACSD data for the uppermost 2-cm increment. The inventory (accumulated mass per unit area) for each site was determined for cores taken after 1989 using dry densities calculated from measured bulk densities, as described above for USGS cores. In years prior to 1991, the measured water content and an assumed particle density (2.65 g/cm^3) were used to calculate bulk density. We expressed temporal trends in the vertical distribution of *p,p′*-DDE based on representative values of the depths of selected points on the *p,p′*-DDE profiles (Table 2). The selected profile points are (1) the location of the peak *p,p′*-DDE concentration, (2) location of the lower shoulder of the profile, defined by a fixed *p,p′*-DDE value (10 ppm at Site 3C and 15 ppm at Sites 6C and 8C) located in the regions of steepest concentration gradient, (3) the deepest point where *p,p′*-DDE concentrations exceed 1 ppm, and (4) the depths at which cumulative mass per unit area

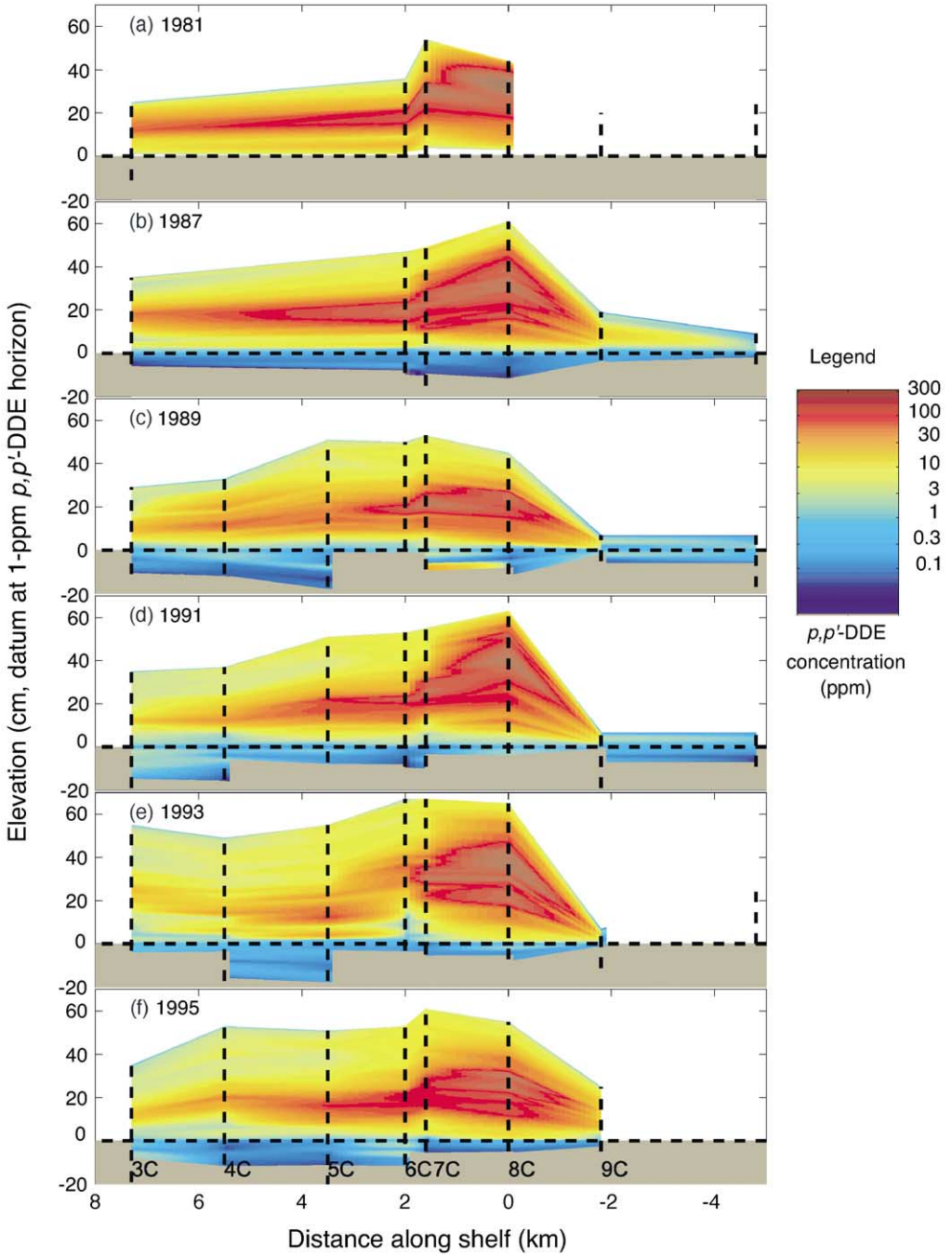

Fig. 7. Contours of LADSD p,p'-DDE concentrations for cores along the 60-m isobath for 6 biennial surveys. Locations of cores are shown with vertical dashed lines; no p,p'-DDE data are available for Sites 9C and 10C in 1981 or Site 10C in 1993, and insufficient data were available to contour 1983 and 1985. Vertical origin of each core has been shifted to the depth where p,p'-DDE first falls below 1 ppm, providing a horizontal datum that approximates the surface of pre-effluent sediment.

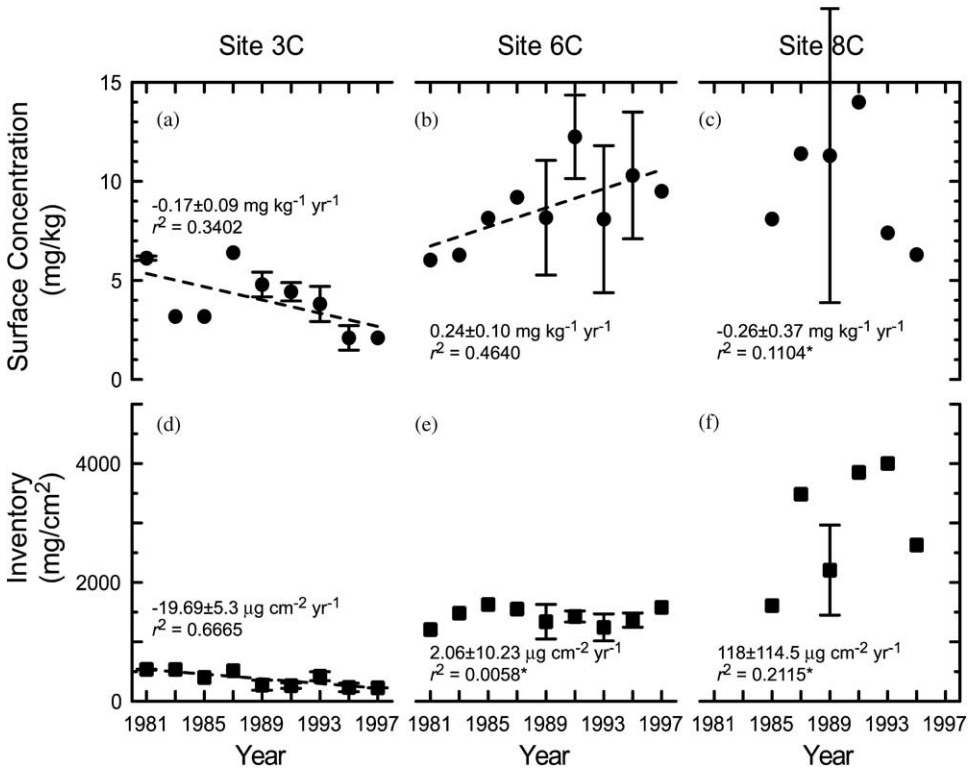

Fig. 8. Time series of surface (top 2 cm) concentrations of *p,p′*-DDE and inventory (total mass of *p,p′*-DDE per unit area of seabed) at Sites 3C, 6C, and 8C. Values are mean of individual replicate cores; error bars indicate the standard deviation among replicates. Least-squares linear fits are plotted for time series with slopes that differ from zero at the 90% confidence level (Table 2).

(integrated from the sediment-water interface downward) are 15%, 50%, and 85% of the total mass per unit area for the core. These points, referred to as C15, C50, and C85, are used to define the width of the normalized mass distribution of the *p,p′*-DDE profile (Fig. 9). We also tracked (Table 2) the depth of dry density thresholds (0.875 g/cm^3 through 1989 and 1.05 g/cm^3 after that date), chosen because they separate bimodal populations of densities associated with the effluent-affected sediment and underlying pre-effluent sediment. The threshold is different after 1989 because the method for determining dry density changed, as discussed above.

Large variations can be found in the LACSD profiles and the representative values we have extracted from them (Figs. 8 and 9, Table 2). Variability among replicates arises from inconsistent core recovery or small-scale (a few meters) spatial variability, while variations between sample years includes both factors and temporal variability. To separate temporal changes in representative values from differences among replicates, we used averages calculated in either of two ways: (1) averages of the representative values for the several replicate cores, or (2) deriving representative values from a single average profile formed by arithmetic averaging of concentrations in each depth interval. Average profiles may combine as many as four replicates near the surface and as few as one near the bottom of the deepest core. We used method (1) to calculate surface concentrations and total inventories and method (2) to calculate the depths of points picked from the profiles. The values differ, but not systematically, and method (2) allows us to initialize and compare models with a single representative profile (Sherwood et al., this issue). In the following discussion,

Table 2
Burial velocities of points on *p,p′*-DDE profiles collected biennially by LACSD

Location	Profile characteristic	Least-squares slope ± standard error (cm yr^{-1})	Coefficient of regression r^2
Site 3C 1981–1997 $N = 9$	Peak depth	0.93 ± 0.16	0.8296
	Lower shoulder depth	0.48 ± 0.28	0.2947
	1 ppm depth	1.55 ± 0.34	0.7508[a]
	Cumulative 15th percentile (C15)	0.22 ± 0.14	0.2543[b]
	Cumulative 50th percentile (C50)	0.86 ± 0.12	0.8761
	Cumulative 85th percentile (C85)	1.09 ± 0.19	0.8252
	Density threshold depth	0.92 ± 0.22	0.7202
Site 6C 1981–1997 $N = 9$	Peak depth	0.65 ± 0.18	0.6512
	Lower shoulder depth	0.48 ± 0.29	0.2803[b]
	1 ppm depth	1.21 ± 0.26	0.7642[c]
	Cumulative 15th percentile	0.36 ± 0.23	0.2672[b]
	Cumulative 50th percentile	0.66 ± 0.19	0.6374
	Cumulative 85th percentile	0.75 ± 0.21	0.6528
	Density threshold depth	0.70 ± 0.34	0.3868
Site 8C 1981, 1983–1995 $N = 6$	Peak depth	1.46 ± 0.62	0.5794
	Lower shoulder depth	1.87 ± 0.66	0.6653
	1 ppm depth	2.10 ± 0.60	0.7566[d]
	Cumulative 15th percentile	0.85 ± 0.34	0.6076
	Cumulative 50th percentile	1.30 ± 0.43	0.6961
	Cumulative 85th percentile	1.58 ± 0.49	0.7171
	Density threshold depth	4.04 ± 0.98	0.8091

Note: Positive slopes (peaks, lower shoulder, etc.) indicate burial. When replicate cores were available, profile points were determined by fitting a line through points picked from the average profile, a profile computed from the mean of replicates at each sampled depth interval.

[a] Four of the 16 cores at Site 3C had values $> 1\,\mathrm{mg\,kg^{-1}}$ in the lowest interval tested.

[b] Slopes are not significantly different from zero at the 90% confidence level.

[c] Four of the 15 cores at Site 6C had values $> 1\,\mathrm{mg\,kg^{-1}}$ in the lowest interval tested.

[d] Two of the seven cores at Site 8C had values $> 1\,\mathrm{mg\,kg^{-1}}$ in the lowest interval tested.

rates are cited as the slope of the least-squares linear fit ± the standard error. Slopes differ significantly from zero at the 90% confidence level unless otherwise noted with an asterisk in Fig. 8 or Tables 2 or 3.

At Site 3C, there has been a nearly monotonic decrease in *p,p′*-DDE inventory, from a maximum of 525 μg/cm^2 in 1981 to 226 μg/cm^2 in 1997 at a rate of $-19.7 \pm 5.3\,\mu\mathrm{g/cm^2/yr}$ over the 16-yr interval. This decrease has been accompanied by a decrease in surface concentrations, which are the lowest of the three sites (Fig. 8, panel a; Table 2), a decrease in maximum concentrations in the *p,p′*-DDE peak (not shown), from 110 ppm in 1981 to 21 ppm in 1997, and a general burial of the mass of *p,p′*-DDE. The depth to the center of mass (C50) increased at an average rate of 0.86 ± 0.12 cm/yr. The profile also has broadened, particularly above the peak, as evidenced by the distances between C50-C15 and C85-C50 (Fig. 9, panel a; Table 3).

Measurements of *p,p′*-DDE at Sites 6C reveal, in contrast, no long-term changes in inventory (Fig. 8, panel e; Table 2). Inventories have varied only about 10% around the long-term mean of 1400 μg/cm^2 and surface concentrations have increased slightly. The mass of *p,p′*-DDE has been buried at 0.66 ± 0.19 cm/yr, more slowly that at either Site 3C or Site 8C. Maximum concentrations in the *p,p′*-DDE peak at Site 6C have been variable, but have generally decreased from a high of 270 ppm in 1985 to 160 ppm in 1995. In the region above the peak, the profile has broadened

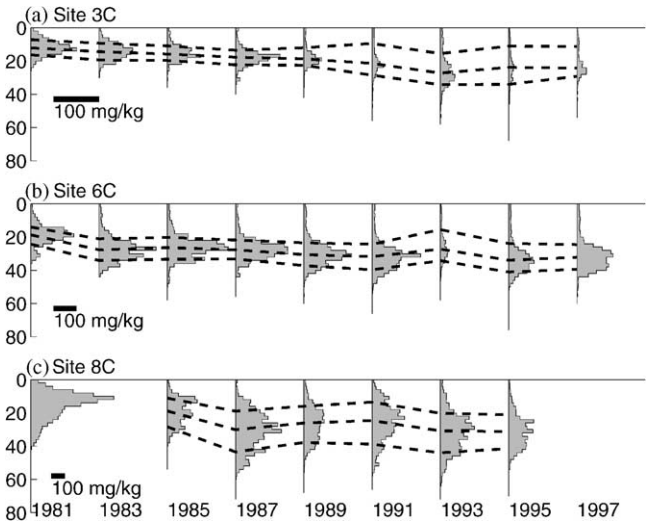

Fig. 9. Time series of p,p'-DDE (shaded regions) for Sites 3C, 6C, and 8C. Dashed lines connect cumulative 15-, 50-, and 85-percentile depths (see text). Note that the scale for p,p'-DDE varies among sites (dark bar scales). No p,p'-DDE data are available for Site 8C in 1983 or 1997.

Table 3
Spreading rates of p,p'-DDE profiles and inferred diffusion coefficients between depths of cumulative 15th and 50th percentiles (C15 and C50), and 50th and 85th percentiles (C50 and C85)

Location	Profile interval	Linear rate from least-squares slope $\pm$standard error (cm yr^{-1})	Coefficient of regression r^2	Estimated diffusion coefficient D (cm^2 yr^{-1})
Site 3C	Upper (C15–C50)	0.64 ± 0.11	0.8164	5.6
	Lower (C50–C85)	0.22 ± 0.12	0.3507	1.2
Site 6C	Upper	0.29 ± 0.10	0.5255	2.3
	Lower	0.09 ± 0.04	0.4310	0.6
Site 8C	Upper	0.45 ± 0.13	0.7388	3.7
	Lower	0.28 ± 0.14	0.4915[a]	3.4[a]

[a] Slope is not significantly different from zero at the 90% confidence level.

but, below the peak, there has been only a slight increase in profile width (Fig. 9, panel b; Table 3).

There are fewer data and greater variability at Site 8C, and no apparent trends in inventory (which is the highest of the three sites, averaging 3000 μg/cm^2, with a wide range of 1610–4000 μg/cm^2) or surface concentration (also the highest of the three sites, averaging 9.8 ppm). Site 8C also has the highest apparent burial rate, with the depth of C50 increasing at 1.30 ± 0.43 cm/yr. The profile has broadened in the region above the peak, and has not changed significantly below the peak (Figs. 8 and 9, Table 3).

The spreading rate of the profiles can be used to derive a first approximation of mixing rates for idealized profiles. Assuming the concentration profiles have a Gaussian shape and are not bounded by interfaces above or below the effluent-affected layer, and assuming a constant, uniform rate of diffusion on either side of the

concentration peak, classical diffusion theory (e.g., Carslaw and Jaeger, 1959; Csanady, 1973) can be used to relate changes in the vertical width of the concentration profile (s) to a diffusion coefficient D as: $s^2 = 2Dt$, where t is time. The distance between the 15th and 50th percentiles (or between the 50th and 85th percentiles) in a Gaussian distribution is $1.034s$ (Sachs, 1984, Table 13), so $D \sim = 0.5\mathrm{d}(x^2)/\mathrm{d}t$, where x is the measured distance between C15 and C85 or between C50 and C85. Least-squares estimates of $\mathrm{d}(x)^2/\mathrm{d}t$ were made from temporal trends of $(\mathrm{C50\text{-}C15})^2$ and $(\mathrm{C85\text{-}C50})^2$ and values for D in the upper and lower portions of the profiles were estimated (Table 3). These values apply to broad and generally increasing depth intervals surrounding C50, which ranged from 11 to 22 cm at Site 3C, from 18 to 33 cm at Site 6C, and from 12 to 29 cm at Site 8C. Values of 5.6, 2.3, and 3.7 cm^2/yr were estimated for the upper portions of profiles at Sites 3C, 6C, and 8C, respectively, which are qualitatively consistent with the observations of Swift et al. (1996), who indicated that effective mixing extended to nearly 20 cm at Site 3C and to nearly 30 cm at Site 6C in ^{210}Pb profiles collected in 1991 (their Fig. 9). The values of the mixing coefficients also seem reasonable when compared to those of Wheatcroft and Martin (1996), which range from 49 to 10 cm^2/yr and apply to the top 5–8 cm.At Sites 3C and 6C, the diffusion coefficient is lower in the lower portion of the profile, and at Sites 8C, the absence of a significant trend in the distance between C50 and C95 suggests that mixing is negligible below C50. A low rate of mixing at depth is consistent with decreasing abundance and biomass of benthic infauna (Swift et al., 1996).

6. Dimensions of the contaminated, effluent-affected sediment deposit

6.1. Dimensions of the effluent-affected sediment layer based on very-high-resolution (chirp) subbottom profiling

The chirp profiling system was used to measure the thickness of the effluent-affected sediment layer (Hampton et al., 2002). There is a large acoustic impedance contrast across the interface between the relatively low density, effluent-affected sediment and the underlying, relatively high-density native sediment (Fig. 10). The energy reflected by this interface produces a discernible signature on chirp profiles. The upper layer can be resolved when it is thicker than about 20 cm (the resolution of the chirp system). The space between the seabed reflector and this subbottom reflector represents the thickness of the effluent-affected layer. Thickness measurements were plotted on a geographic reference grid and hand contoured at a 10-cm interval. Thickness values were obtained over an area of 10.8 km^2. Integration of these values yields a volume of about 3.2 million m^3 of effluent-affected sediment (Hampton et al., 2002).

6.2. Dimensions of the effluent-affected layer based on variations in core physical properties

Cylindrical core samples taken by the USGS were logged for acoustic velocity, magnetic susceptibility, and bulk density using the gamma ray attenuation method (Kayen et al., 1999). Measured values were obtained at 1-cm spacing before the cores were split or otherwise processed, yielding a nearly continuous, non-destructive description of the lithology of the cores. The presence of effluent-affected sediment commonly produces a layer of relatively low density that coincides with the layer of sediment that is most contaminated with *p,p′*-DDE (Fig. 10). All of the density logs were assessed to estimate the thickness of the effluent-affected sediment layer at each coring station. Fig. 11 is an isopach map of the effluent-affected sediment deposit based on an assessment of our density profiles. An integration of the volume of the deposit, as shown in Fig. 11, yields 9.8 million m^3. Sixty-eight percent of the volume is on the shelf in water depths shallower than 100 m and 32% is on the slope. Note that these volumes are lower bounds because some of the cores did not penetrate all the way through the effluent-affected sediment deposit and some effluent-affected sediment lies beyond the area mapped.

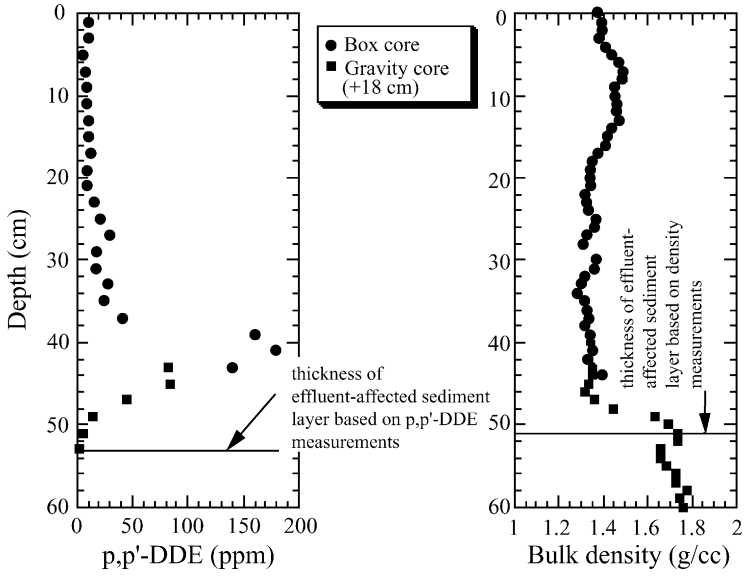

Fig. 10. Density and *p,p′*-DDE profiles at Station 556 (See Fig. 2 for location), illustrating that the base of the layer impacted by *p,p′*-DDE and the base of the low density effluent-affected sediment layer are comparable.

6.3. Dimensions of the effluent-affected layer based on geostatistical interpretation of a data set that combines thicknesses from chirp profiles and density logs

Murray et al. (2002), present the results of a geostatistical study that evaluates the geometry of the effluent-affected sediment layer using a data set that combines thicknesses from chirp profiling and interpretation of density logs from cores. Variograms (Isaaks and Srivastava, 1989) were used to analyze the spatial continuity of the thickness data, and showed the presence of strong spatial continuity, with the maximum direction of continuity parallel to the shoreline. The variogram range of the thickness data in the alongshore direction was 1400 m, which indicates the presence of a large, continuous body of effluent-affected sediment. The variogram model was used as input to a conditional sequential simulation program that produced 100 equiprobable maps of the distribution of the thickness of the effluent-affected layer. These maps were analyzed statistically to obtain the expected values of the distribution of thickness at regularly spaced grid nodes in the map area (Murray et al., 2002). The maps of the expected values were integrated to yield a total volume of 7.8 million m^3 over an area of 22.1 km^2. The geostatistical mapping indicated that the effluent-affected sediment is thick near the outfall pipes, and immediately northwest of the outfall pipes along the 60 m isobath.

6.4. Dimensions of the effluent-affected sediment layer based on USGS p,p′-DDE profiles

Estimates of the thickness of sediment impacted by *p,p′*-DDE were made using plots of *p,p′*-DDE vs. depth in the sediment (e.g., Fig. 10). For cores in which *p,p′*-DDE measurements are available, a good correspondence between the thickness of the effluent-affected sediment layer based on density logs and the thickness of the effluent-affected sediment layer based on *p,p′*-DDE profiles is typically obtained (Fig. 12, correlation coefficient, *R*, of 0.96). If only the upper part of the effluent-affected sediment layer were contaminated with DDT, the layer thickness estimated from *p,p′*-DDE profiles would be less than that determined from density profiles. Accordingly, these results illustrate that virtually the entire effluent-affected sediment layer is contaminated with DDT. There

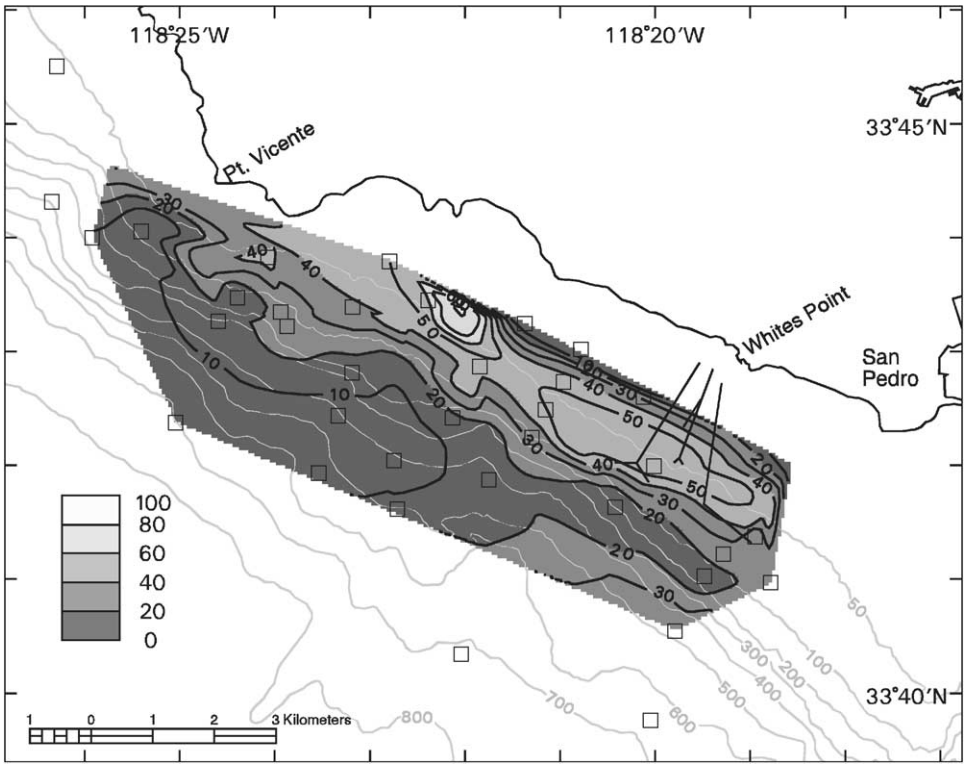

Fig. 11. Thickness (in cm) of the effluent-affected sediment layer determined from density logs of cores. Table 1 shows the integrated volume of the effluent-affected sediment layer as a function of water depth.

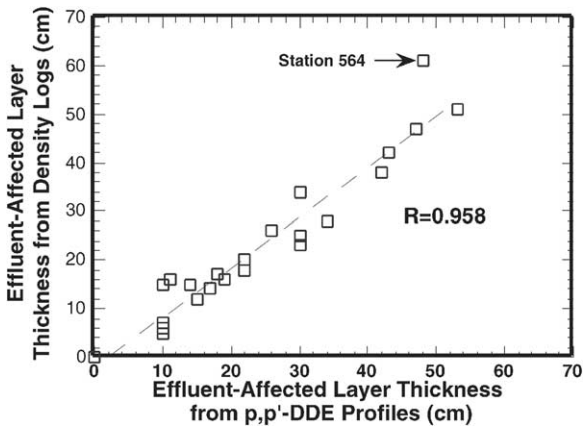

Fig. 12. Comparison of the thickness of the effluent-affected sediment layer determined from density logs and *p,p′*-DDE profiles.

is a tendency for the thickness obtained from *p,p′*-DDE profiles to be about 2 cm greater than that obtained from density measurements, probably because bioturbation mixes *p,p′*-DDE into native sediment. Thus, the thicknesses and volumes of the layer obtained from density logs are conservative estimates of the thickness and volume of contaminated sediment.

At only one station (564, very near the diffuser pipes) did the thickness of the effluent-affected sediment layer determined from density logs significantly exceed (by 13 cm) the thickness of the effluent-affected sediment layer determined from *p,p′*-DDE profiles (Fig. 12). At this station, the low density sediment located below sediment heavily impacted by *p,p′*-DDE is probably sediment affected by effluent before the introduction of significant DDT to this environment. Given that station 564 is the USGS station nearest the outfall pipe, this finding may show that an areally limited, effluent-affected deposit existed near the outfall before the introduction of significant DDT. Because only one station shows this characteristic, either the size of that deposit was small or, if such

Table 4
Comparison of the volumes and mass of the effluent-affected sediment layer during the 1992 USGS surveys, estimated by different means

Water depth (m)	Volume (million m^3)-from chirp profiling-(Area = 10.8 km^2)	Volume (million m^3)-from density logs-(Area = 39.5 km^2)	Expected volume (million m^3)-from geostatistical analysis-(combined chirp and density log data)(Area = 22.1 km^2)	Dry mass (million metric tons)-from density logs-(effluent-affected layer) (Area = 39.5 km^2)
30–60		4.3	6.6	2.9
60–100		2.3		1.7
100–200		0.8		0.6
200–400		1.2	1.2	0.8
>400		1.2		0.3
Total	3.2	9.8	7.8	6.3

a deposit originally existed at other stations, it has since become contaminated by downward mixing.

6.5. *Comparison of dimensions of the effluent-affected sediment layer, determined using different procedures*

Table 4 shows a compilation of comparable effluent-affected sediment layer characteristics. The total volume determined by chirp profiling is least (3.2 million m^3), because only a small area (Hampton et al., 2002) could be effectively surveyed, given the limitations of the chirp system. Within that area, however, the effluent-affected layer thicknesses are comparable to those obtained using LACSD or USGS cores. The geostatistical study, which combines thicknesses from chirp and density logs gives a nearly identical volume on the shelf to those from cores (both yielding 6.6 million m^3). The volume on the slope from the geostatistical study is less than those from other methods, probably because the area considered does not continue as far down the slope.

7. Summary and conclusions

Measurements by the USGS and the sanitation districts of Los Angeles County (LACSD) provide a quantitative description of the distribution of DDT and its byproducts and effluent-affected sediment on the Palos Verdes margin. A 5-cm to greater than 50-cm-thick effluent-affected-sediment deposit extends over most of the shelf and slope between Point Fermin and Point Vicente. Association of the sediment body with effluent discharged from the Whites Point outfall is illustrated by high concentrations of organic carbon and increased thickness and contamination levels near the outfall. The effluent-affected deposit is generally <70-cm thick, has a volume of about 10 million m^3, and is spread over an area of about 40 km^2. About 70% of the volume of the deposit is present in water depths <100 m, which primarily constitutes the continental shelf. Geostatistical analysis showed strong spatial continuity of the deposit, especially in the alongshore direction. In cores, the effluent-affected layer commonly exhibits lower density and higher water content than the underlying native silty sands, and is thus easily distinguished. Along the 60-m isobath, the deposit comprises two units: (1) a lower unit (centimeters to tens of centimeters thick) of organic-rich, fine-grained sediment with high concentrations of DDT and PCBs, and (2) an overlying relatively less-contaminated layer of organic-rich sediment ranging in thickness from a few centimeters on the continental slope to about 20–30 cm on parts of the shelf (Figs. 4 and 7). The deeper, more contaminated unit was produced between 1950 and the early 1970s, a period when

discharges of all contaminants, including DDT, PCBs and heavy metals, were essentially uncontrolled and the annual suspended sediment emissions of the JWPCP system increased dramatically (Fig. 3). The upper unit is generally less contaminated, and formed since 1970, when source control and improved treatment strategies were instituted. These strategies led to rapid and substantial decreases in the discharges of most contaminants and suspended particulates (Fig. 3).

Virtually all of the effluent-affected sediment deposit is contaminated with DDT and PCBs. The dominant isomer of DDT, *p,p′*-DDE, can be used as a proxy for mapping total DDT and total PCBs, given excellent correlations between total DDT and *p,p′*-DDE, and between total PCBs and *p,p′*-DDE (correlation coefficients of 0.97 and 0.99, respectively; Murray et al., this issue). The footprint of DDT-contaminated sediment, delimited at the 1 ppm *p,p′*-DDE concentration level in the upper 4-cm of the sediment column covers a seafloor surface area in excess of 40 km^2. At the 5 ppm *p,p′*-DDE concentration level, an area in excess of 12 km^2 is covered; and at the 10 ppm *p,p′*-DDE concentration level, an area of 3.4 km^2 is covered near the Whites Point outfall. The maximum concentration of *p,p′*-DDE exceeds 200 ppm near the outfall pipes; maximum concentrations in excess of 50 ppm extend up to 4 km to the west of the outfalls. The total mass of *p,p′*-DDE that has been retained on the margin is greater than 66 mt (metric tons). About 75% of the total mass is present in water depths <100 m.

Evaluation of temporal trends for three LACSD stations along the 60-m isobath showed that changes at the most distal station (Site 3C) were markedly different from changes at Sites 6C and 8C, which are both closer to the outfalls and contain significantly higher inventories of *p,p′*-DDE. At Site 3C, there has been about a 50% reduction in *p,p′*-DDE inventory during a 16-yr period, accompanied by a decrease in peak concentrations and a broadening of the mass distribution profile. At Site 6C, the *p,p′*-DDE inventory has not fallen significantly during the same period, peak concentrations have fallen slightly, surface concentrations have increased, and the peak width has broadened slightly, mostly in the upper portion. At Site 8C, there has been no significant changes in inventory, surface concentrations, or peak concentrations, but there is some evidence of profile broadening in the upper portion.

Given that inventories of *p,p′*-DDE have not fallen to any great extent over 16 years at stations 6C and 8C, we conclude that degradation and sediment transport processes are not having a strong effect in removing *p,p′*-DDE contamination from the most impacted part of the deposit. Processes at 3C, a distal, less impacted station, appear to be removing *p,p′*-DDE from the sediment column at a moderate rate. As discussed by Eganhouse et al. (2000), likely mechanisms for this reduction include physical and biologically mediated remobilization.

Acknowledgements

This study was jointly funded by the US Geological Survey and the National Oceanic and Atmospheric Administration as part of a study to examine the potential for natural recover of contaminated sediment near the Whites Point Outfall. We would like to thank William McArthur, Helder Costa, Robert Kayen, Jan Stull, Michael Torresan, Robert Eganhouse, Kevin O'Toole, Walter Olsen, Tisha Clark, Eran Hayden, Larry Phillips, John Chen, Thomas Chase, and the crew and officers of the R/V Farnella for their support during the various stages of this study. The manuscript benefited from helpful reviews by Monty Hampton and two anonymous reviewers.

References

Bascomb, W., Mardesich, A.J., Stubbs, H., 1982. An improved corer for soft sediments. SCCWRP Annual Report (1981–82), pp. 267–271.

Brownlie, W.R., Taylor, B.D., 1981. Coastal sediment delivery by major rivers in Southern California. In: Sediment Management of Southern California Mountains, Coastal Plains, and Shorelines, Part C. Environmental Quality laboratory Report 17-C. California Institute of Technology, Pasadena, CA.

Carslaw, H.S., Jaeger, J.C., 1959. Conduction of Heat in Solids. Oxford University Press, London.

Conrad, C.L., Ehlig, P.L., 1987. The monterey formation of the Palos Verdes Peninsula, California: an example of sedimentation in a tectonically active basin within the California Continental Borderland. Geology of the Palos Verdes Peninsula and San Pedro Bay, Pacific Section, Society of Economic Paleontologists and Mineralogists, pp. 17–30.

Csanady, G.T., 1973. Turbulent Diffusion in the Environment. D. Reidel Publishing Company, Dordrecht, Holland, 248pp.

Eganhouse, R.P., Pontolillo, J., Leiker, T.J., 2000. Diagenetic fate of organic contaminants on the Palos Verdes shelf, California. Marine Chemistry 70, 289–315.

Emery, K.O., 1960. The Sea Off Southern California—A Modern Habitat of Petroleum. Wiley, New York, 366pp.

Fischer, P.J., Lee, C.F., 1992. Evolution of the Santa Monica-San Pedro Margin, California during the last 25,000 years. In: Heath, E.G., Lewis, W.L. (Eds.), The Regressive Pleistocene Shoreline of Southern California, Annual Field Trip Guide Book No. 20. South Coast Geological Society, Inc.

Gardner, J.V., Dartnell, P., Mayer, L.A., Hughes Clark, J.E., 1999a. Shaded-relief bathymetric and backscatter maps of Santa Monica margin, California. USGS Geologic Investigation Series I-2648 (2 sheets).

Gardner, J.V., Hughes Clark, J.E., Mayer, L.A., 1999b. High resolution multibeam bathymetry of the San Pedro Shelf region, southern California. USGS Open-File Report 99–360.

Hampton, M.A., Lee, H.J., Locat, J., 1996. Submarine landslides. Reviews of Geophysics 34, 33–59.

Hampton, M.A., Murray, C.J., Karl, H.A., 2002. Acoustic profiles, images of the Palos Verdes margin: implications concerning deposition from the Whites Point outfall. Continental Shelf Research 22, 841–857.

Hickey, B.M., 1992. Circulation over the Santa Monica-San Pedro basin and shelf. Progress in Oceanography 30, 37–115.

Inman, D.L., Jenkins, S.A., 1999. Climate change and the episodicity of sediment flux of small California rivers. The Journal of Geology 107, 251–270.

Isaaks, E., Srivastava, R.M., 1989. An Introduction to Applied Geostatistics. Oxford University Press, New York.

Kayen, R.E., Phi, T., 1997. Using HyperCard for robotic control and data collection. Scitech Journal 7, 24–29.

Kayen, R.E., Edwards, B.D., Lee, H.J., 1999. Nondestructive laboratory measurement of geotechnical and geoacoustic properties through intact core-liner. In: Marr, W.A., Fairhurst, C.E. (Eds.), Nondestructive and Automated Testing for Soil and Rock Properties, ASTM STP 1350. American Society for Testing and Materials, West Conshohocken, PA, pp. 83–94.

Kayen, R.E., Lee, H.J., Hein, J.R., 2002. Influence of the Portuguese bend landslide on the character of the effluent-affected sediment deposit, Palos Verdes margin, southern California. Continental Shelf Research 22, 911–922.

Kolpack, R.L., 1987. Environmental processes affecting DDT contaminated sediments off Palos Verdes, California: A sediment dynamics workshop sponsored by the LACSD. County Sanitation Districts of Los Angeles County (LACSD), Los Angeles, CA, 102pp.

LACSD (Sanitation Districts of Los Angeles County), 1992. Palos Verdes Ocean monitoring: sediment Report 1992. Annual Report, Sanitation Districts of Los Angeles County, Whittier, CA.

LACSD (Sanitation Districts of Los Angeles County), 1998. Annual Report 1998: Palos Verdes Ocean monitoring. Sanitation Districts of Los Angeles County, Whittier, CA.

Lambe, T.W., Whitman, R.V., 1969. Soil Mechanics. Wiley, New York, 553pp.

Lee, H.J., Locat, J., Dartnell, P., Minasian, D., Wong, F., 2000. A GIS-based regional analysis of the potential for shallow-seated submarine slope failure. Proceedings of the Eighth International Symposium on Landslides. Cardiff, Wales, June, 2000.

Merriam, R., 1960. Portuguese bend landslide, Palos Verdes Hills, California. Journal of Geology 68, 140–153.

Moore, D.G., 1960. Acoustic-reflection studies of the continental shelf and slope off southern California. Geological Society of America Bulletin 71, 1121–1136.

Murray, C.J., Lee, H.J., Hampton, M.A., 2002. Geostatistical mapping of effluent-affected sediment distribution on the Palos Verdes shelf. Continental Shelf Research 22, 881–897.

Noble, M.A., Ryan, H.F., Wiberg, P.L., 2002. The dynamics of subtidal poleward flows over a narrow continental shelf, Palos Verdes, California. Continental Shelf Research 22, 923–944.

Pierson, L.J., Schiller, G.I., Slater, R.A., 1987. Archaeological resource study: Morro Bay to Mexican border. Final report to US Minerals Management Service, Department of the Interior, 199pp.

Rice, R.M., Gorsline, D.S., Osborne, R.H., 1976. Relationships between sand input from rivers and the composition of sands from the beaches of southern California. Sedimentology 23, 689–703.

Rosfelder, A.M., Marshall, N.F., 1967. Obtaining large, undisturbed, and oriented samples in deep water. In: Richards, A.F. (Ed.), Marine Geotechnique. University of Illinois Press, Champaign, IL, pp. 243–263.

Sachs, L., 1984. Applied Statistics, Second Edition. Springer, Berlin, 707pp.

Sherwood, C.R., Drake, D.E., Wiberg, P.L., Wheatcroft, R.A., 2002. Prediction of the fate of DDT in sediment on the Palos Verdes margin. Continental Shelf Research 22, 1025–1058.

Stull, J.K., Swift, D.J.P., Niedoroda, A.W., 1996. Contaminant dispersal on the Palos Verdes continental margin: sediments and biota near a major California wastewater discharge. The Science of the Total Environment 179, 73–90.

Swift, D.J.P., Stull, J.K., Niedoroda, A.W., Reed, C.W., Wong, G.T.F., 1996. Contaminant dispersal on the Palos Verdes continental margin II. Estimates of the biodiffusion coefficient D_b, from composition of the benthic infaunal community. The Science of the Total Environment 179, 91–107.

Wheatcroft, R.A., Martin, W.R., 1996. Spatial variation in short-term (Th-234) sediment bioturbation intensity along an organic carbon-gradient. Journal of Marine Research 54, 763–792.

Wong, F., 2002. Heavy mineral provinces of the Palos Verdes margin, southern California. Continental Shelf Research 22, 899–910.